VOLUME 1, NUMBER 11, NOVEMBER 2001

NANO LETTERS

Nanoclusters of Iridium Oxide and of Rhodium Oxide Supported on MgO

F. S. Lai and B. C. Gates*

Department of Chemical Engineering and Materials Science, University of California, Davis, California 95616

Received July 25, 2001; *Revised Manuscript Received August 15, 2001*

ABSTRACT

MgO-supported Ir_4 and Rh_6, prepared from $[Ir_4(CO)_{12}]$ and $[Rh_6(CO)_{16}]$, respectively, on MgO, were partially oxidized at 323 K, with partial destruction of the metal frames, and reformed by treatment in H_2. Oxidation at higher temperatures resulted in total oxidation of the clusters with breakup of the metal frames, and treatment in H_2 led to near reconstruction of the metal clusters, but with some migration and aggregation. The results imply that the oxidized nanoclusters were site isolated on the support surface; this is the first report of oxide clusters of noble metals. The metal oxide clusters are catalytically active for CO oxidation.

Nanoclusters or nanoparticles dispersed on porous supports are the common form of solid catalyst, offering the advantages of high surface area per unit volume of the catalyst and a large fraction of the catalytically active material at surfaces, where it is accessible to reactants. Typical catalysts for oxidation reactions are metal oxides and noble metals, and the latter, in operation, typically consist of nanoparticles of metal covered in part with surface oxide layers. Gas-phase oxide nanoclusters[1] have been investigated as structurally well-defined models of oxidation catalysts, but these have been restricted to oxides of nonnoble metals. Supported nanoclusters of noble metals have been thoroughly investigated,[2−4] but there are only few reports of supported nanoclusters of metal oxides, and these are oxides of non-noble metals (Fe,[5] Mo,[6] and W[7]) supported in zeolites. We now report oxide nanoclusters of noble metals dispersed on oxide supports and their catalytic performance for oxidation of CO.

The supported samples were prepared with standard air-exclusion techniques by formation of nanoclusters of metal on a high-area MgO support followed by oxidation to convert the metal nanoclusters into metal oxide nanoclusters. The supported nanoclusters Ir_4/MgO and Rh_6/MgO were prepared from the precursors $[Ir_4(CO)_{12}]$ (Strem, 98%) and $[Rh_6(CO)_{16}]$ (Strem, 98%), respectively. Rh_6/MgO was synthesized by adsorption of $[Rh_6(CO)_{16}]$ on MgO calcined at 673 K (MgO_{673}), followed by decarbonylation in He at 573 K; Ir_4/MgO was synthesized by adsorption of $[Ir_4(CO)_{12}]$ on MgO_{973} followed by decarbonylation in He at 593 K. The methods are described elsewhere.[2,8−10] The decarbonylated samples were pretreated in H_2 at 573 K prior to oxidation and reduction treatments. Reagent-grade *n*-hexane (Aldrich), used as a solvent to bring the metal carbonyl precursors in contact with the support, was dried over sodium benzophenone ketyl. MgO powder (97%, EM Science) was used as received. The BET surface area of MgO_{673} was approximately 60 $m^2\ g^{-1}$,[11] and that of MgO_{973} was approximately 18 $m^2\ g^{-1}$.[2] The treatment gases used in the sample preparations were He (Matheson, 99.999%, purified by passage through traps to remove traces of O_2 and moisture) and H_2 (Matheson, 99.999%, or generated by electrolysis of

* Corresponding author e-mail: bcgates@ucdavis.edu

10.1021/nl0155882 CCC: $20.00
Published on Web 10/23/2001

Table 1: EXAFS Fit Parameters Characterizing MgO-Supported Samples Prepared from $[Rh_6(CO)_{16}]$ and from $[Ir_4(CO)_{12}]$ Prior to Treatments (samples scanned at 77 K under vacuum (pressure $< 10^{-5}$ Torr))[a]

	$[Rh_6(CO)_{16}]/MgO$[b]				$[Ir_4(CO)_{12}]/MgO$[c]			
backscatterer	N	R [Å]	$10^3 \times \Delta\sigma^2$ [Å^2]	ΔE_0 [eV]	N	R [Å]	$10^3 \times \Delta\sigma^2$ [Å^2]	ΔE_0 [eV]
metal (Rh or Ir)								
1st shell	3.8	2.77	6.3	0.0	3.0	2.72	3.4	0.3
2nd shell	0.7	3.84	8.5	7.3				
CO								
C (terminal)	1.0	1.90	−4.4	−5.8	0.8	1.86	−4.3	−6.1
C (bridging)	1.0	2.00	−4.7	13.6				
O	1.9	3.03	5.1	−13.5	0.7	3.01	−5.3	−1.2
support								
O					1.1	2.14	2.4	−13.5
Mg	0.3	3.47	−4.1	2.2				

[a] Notation: N, coordination number; R, absorber-backscatterer distance; $\Delta\sigma^2$, Debye−Waller factor; and ΔE_0, inner potential correction. The approximate experimental uncertainties are as follows: N, ±15%; R, ±0.02 Å; $\Delta\sigma^2$, ±20%; and ΔE_0, ±20%. [b] Results for MgO-supported $[Rh_6(CO)_{16}]$ from literature.[10] [c] Ir−C coordination number for MgO-supported sample made from $[Ir_4(CO)_{12}]$ is less than the value of 3 for $[Ir_4(CO)_{12}]$; evidently, partial decarbonylation took place during the preparation stage.

water in a Balston generator (99.99%)) and purified by flow through traps. The reactant gases used in the catalysis experiments were CO and O_2 in He (Sierra Airgas, Research grade, <0.1% contaminant), purified by passage through a trap containing particles of zeolite 4A to remove traces of water; CO was further purified by flow through a trap of activated γ-Al_2O_3 particles to remove any traces of metal carbonyls from the high-pressure gas cylinder. Each supported catalyst sample contained 1.0 wt % Ir or Rh.

The solid samples were characterized by X-ray absorption spectroscopy at beamline X-11A of the National Synchrotron Light Source (NSLS) at Brookhaven National Laboratory, Upton, NY, and on beamline 2-3 of the Stanford Synchrotron Radiation Laboratory (SSRL) at Stanford Linear Accelerator Center, Stanford, CA. Experimental procedures are as described.[2,3] Data analysis was performed with experimentally and theoretically determined reference files; preparation of the EXAFS reference files is described separately,[12−16] as are the details of the analysis procedures.[16−18]

CO oxidation catalysis was carried out in a once-through tubular flow reactor at atmospheric pressure; reactor temperatures ranged from 298 to 573 K. In a drybox, the catalyst powder (typically, 20−45 mg) was mixed with particles of inert α-Al_2O_3 in a 1:40 ratio by mass and loaded into the reactor. The catalyst bed was held in the middle of the reactor by glass wool plugs. The loaded reactor was inserted into the flow system so that the catalyst did not come into contact with air. The reactant mixture (He + CO + O_2) was purified by traps and fed to the reactor at a constant rate in each catalysis experiment. Total feed flow rate was typically 100 mL (NTP) min^{-1}. Under these conditions, the reactor functioned nearly as an isothermal plug flow reactor. Typical reaction experiments were done with a CO partial pressure of 11 Torr and an O_2 partial pressure of 11 Torr.

An on-line gas chromatograph (Hewlett-Packard, HP-5890 Series II) equipped for column switching in combination with two-channel detection (thermal conductivity detector and flame-ionization detector) was used to separate H_2O from the other product gases on a polar column (Hayesep Q, 8′ × 1/8″, 80−100 mesh), followed by separation of O_2, CO, and CO_2 in a zeolite 5A column (Chrompack, PLOT fused silica, 25-m × 0.53-mm). The conversions were determined with an accuracy of about ± 5%.

The catalysts were characterized by EXAFS spectroscopy before and after decarbonylation and subsequent treatments in O_2. The data (Tables 1−3) show that the decarbonylation of the supported precursor metal carbonyls left the cluster frames essentially intact, as expected,[2,10] as shown by the values of the Ir−Ir and Rh−Rh first-shell coordination numbers of nearly 3 (3.3) and nearly 4 (3.8), respectively, and the lack of higher shell metal−metal contributions, corresponding to the values for the tetrahedral metal frame of $[Ir_4(CO)_{12}]$ and the octahedral metal frame of $[Rh_6(CO)_{16}]$, respectively.

The EXAFS data show that treatment of Ir_4/MgO in O_2 at 323 K and atmospheric pressure led to oxidation of the clusters, as shown by the increased Ir−O contributions in the EXAFS spectra at a distance of about 2.1 Å, in addition to those characterizing the Ir−$O_{support}$ interface (and present in the spectra of Ir_4/MgO prior to treatment in O_2). The oxidation was accompanied by a partial breakup of the Ir_4 tetrahedra, as indicated by the decrease in the Ir−Ir coordination number from 3.2 to 1.3. Treatment of the oxidized and fragmented clusters in H_2 at 573 K and atmospheric pressure led to reconstitution of the tetrahedral Ir_4 clusters, as indicated by the return of the Ir−Ir coordination number to nearly 3.0 and a removal of oxygen, as indicated by the decrease of the Ir−O coordination number (Table 2).

When Ir_4/MgO was treated in O_2 at a higher temperature (523 K), the clusters were oxidized and more completely fragmented, as shown by the EXAFS data (Table 2) indicating an increase in the Ir−O coordination number and the disappearance of the Ir−Ir nearest-neighbor contributions. There were Ir−O contributions at two distances, 1.91 Å, similar to the value for Ir−O in bulk IrO_2, and 2.07 Å, indicating bonding of Ir (and other platinum-group metals in nanoclusters) with the support.[19] Treatment of the fragmented sample with H_2 at 573 K and atmospheric pressure essentially led to reconstruction of the original Ir_4 clusters, except that there is evidence of a small second-shell Ir−Ir

Table 2: EXAFS Fit Parameters Characterizing MgO-Supported Ir_4 after Various Treatments (samples scanned at 77 K under vacuum (pressure $< 10^{-5}$ Torr))[a]

treatment (gas/temperature, K)	absorber-backscatterer pair							
	Ir−Ir				Ir−O			
	N	R [Å]	$10^3 \times \Delta\sigma^2$ [Å^2]	ΔE_0 [eV]	N	R [Å]	$10^3 \times \Delta\sigma^2$ [Å^2]	ΔE_0 [eV]
He/593	3.3	2.61	6.5	−0.9	1.6	2.05	4.2	1.0
					0.4	3.07	−8.0	4.1
He/593; H_2/573	3.2	2.63	4.3	−2.1	1.0	2.10	2.1	−4.3
					1.9	3.41	−2.7	−10.0
He/593; H_2/573; O_2/323	1.3	2.65	3.7	−9.8	2.1	2.08	0.2	0.6
					1.6	2.59	1.8	3.9
He/593; H_2/573; O_2/323; H_2/573	2.9	2.63	2.2	−0.3	1.0	2.06	1.7	1.8
					0.3	2.57	−9.9	−2.0
He/593; H_2/573; O_2/523	none				2.0	1.91	3.6	−9.3
					3.5	2.07	0.1	−1.8
					1.1	3.10	−4.7	−3.8
He/593; H_2/573; O_2/523; H_2/573	3.2	2.69	2.3	−9.7	0.9	2.10	−0.4	−8.4
	0.9	3.79	2.4	−5.1	0.7	3.05	−6.0	2.1

[a] Notes: Notation as in Table 1. There is also evidence of Ir−Mg contributions, but these are not shown, because they are difficult to determine accurately.

Table 3: EXAFS Fit Parameters Characterizing MgO-Supported Rh_6 after Various Treatments (samples scanned at 77 K and $< 10^{-5}$ Torr)[a]

treatment (gas/temperature, K)	absorber-backscatterer pair							
	Rh−Rh				Rh−O			
	N	R [Å]	$10^3 \times \Delta\sigma^2$ [Å^2]	ΔE_0 [eV]	N	R [Å]	$10^3 \times \Delta\sigma^2$ [Å^2]	ΔE_0 [eV]
He/593	3.8	2.66	8.2	11.0	1.3	2.06	1.8	9.6
					0.9	3.16	−3.7	8.9
He/593; H_2/573	4.0	2.67	3.5	3.3	1.3	2.12	3.3	−12.8
	0.9	3.80	2.8	−0.2	0.2	3.23	−10.0	−6.9
He/593; H_2/573; O_2/323	1.0	2.66	4.8	6.0	3.9	2.04	0.5	2.0
					0.5	2.97	−10.0	−11.6
He/593; H_2/573; O_2/323; H_2/573	3.8	2.65	6.9	12.2	2.0	2.00	−4.4	−1.4
					0.3	3.64	−11.7	−8.7
He/593; H_2/573; O_2/448	none				5.0	2.04	−1.9	0.6
					0.8	2.90	−9.8	−9.8
He/593; H_2/573; O_2/448; H_2/573	4.0	2.69	5.5	2.9	1.3	2.05	0.7	−6.9
	0.8	3.80	5.1	−0.4	2.5	3.16	3.8	0.3
	1.0	4.67	2.2	3.8				

[a] Notes: Notation as in Table 1. A second-shell Rh−Rh contribution would be expected for octahedral Rh_6, but it was not always found. The result is as expected, because the imprecision of the higher-shell data usually makes this shell undiscernible within the experimental uncertainty in supported Rh_6.

contribution (at a distance of 3.79 Å) indicating a small degree of aggregation of the clusters on the support; the Ir−O contributions returned to values similar to those characterizing the original supported Ir_4 (Table 2).

Data summarized in Table 3 indicate similar reversible oxidation with partial fragmentation of Rh_6/MgO as a result of treatment in O_2 at 323 K. Treatment in O_2 at 448 K resulted in more complete fragmentation of the Rh_6, with an increase in the Rh−O coordination number and the disappearance of the Rh−Rh nearest-neighbor contributions. The Rh−O contributions do not distinguish between bonds in structures similar to that of the known stable form of rhodium oxide, Rh_2O_3, and Rh−support-oxygen bonds, because the corresponding distances are nearly the same. Reconstruction of the Rh_6 octahedra from the more completely fragmented and oxidized clusters by treatment in H_2 was accompanied by some migration and aggregation of the clusters, as indicated by the third-shell Rh−Rh contribution (Table 3).

The striking result is that the metal clusters were largely reconstructed after they had been oxidized and fragmented. Only if the oxidized species had been site-isolated with the same numbers of metal atoms as the precursor metal clusters would they have been expected to give back the original metal clusters upon reduction. Thus, we infer that the oxidized samples consisted of supported nanoclusters of the oxides of Ir_4 and of Rh_6, containing four and six metal atoms, respectively. What is not clear from the data is whether the metal−metal bonds in the original metal clusters were all broken as a result of the more complete oxidation. The supported oxide clusters might be described as nanoensembles of mononuclear metal oxide complexes near each other but not bonded to each other, but, alternatively, they might be described as oxide nanoclusters that retain some

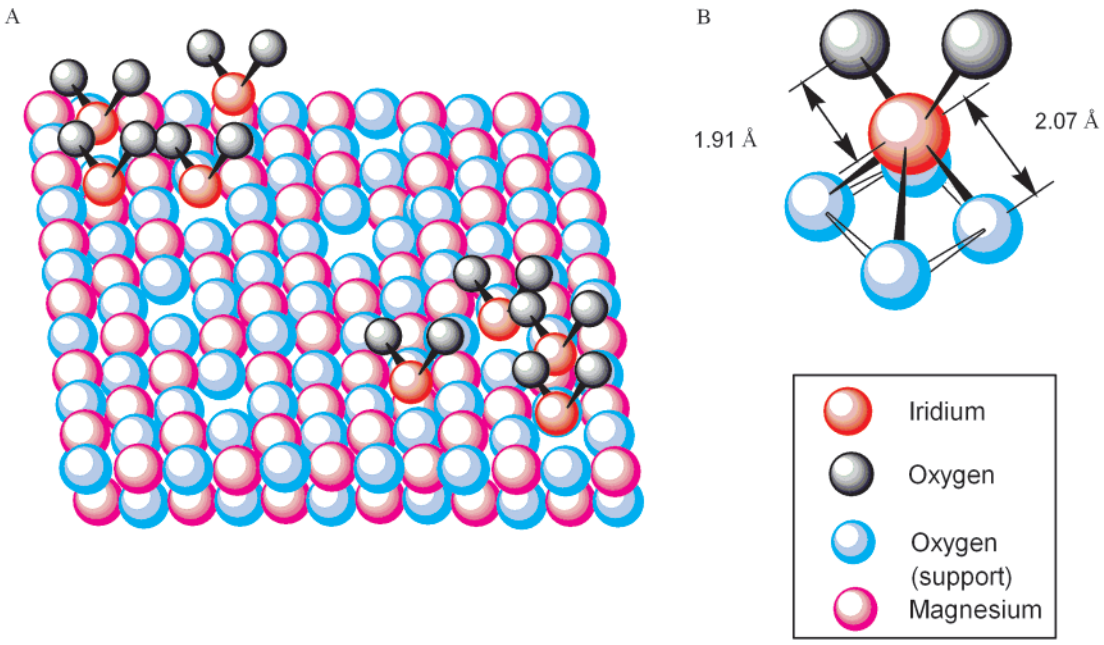

Figure 1. Schematic representation of site-isolated iridium oxide clusters made by oxidizing Ir_4 supported on MgO at 523 K. The dimensions and coordination numbers correspond to the EXAFS data, as described in the text. (A) Site-isolated oxide clusters. (B) Detail showing the Ir−support interaction; this is shown at a cation defect site, where the metal is expected to be more strongly bonded than at a defect-free site.[20]

metal−metal bonds or structures in which oxygen atoms bridge neighboring metal atoms to hold them together. If there were oxide nanoclusters with metal−metal bonds, they would have to be disordered to account for the lack of metal−metal contributions in the EXAFS spectra.

The structures of the supported iridium oxide clusters are represented schematically in Figure 1, which was constructed to match the EXAFS data representing the more fully fragmented clusters, assuming that all the metal−metal bonds were broken. Each iridium atom is depicted as bonded to an average of four oxygen atoms of the MgO surface (the data are fitted as well by three of these oxygen atoms) and by two additional oxygen atoms, with the distances being the EXAFS values. This structure is accommodated by the predominant (001) face of MgO. It is expected on the basis of theoretical results that bonding would be much stronger at cation defect sites than on the simple (001) face.[20] (Similar structures on other faces of MgO or at defect sites would accommodate three oxygen atoms of the support per Ir atom.)

The samples consisting initially of the decarbonylated supported metal clusters, on one hand, and the supported metal oxide clusters, on the other, were tested as catalysts for CO oxidation. The results (Figure 2) indicate that all the samples show ignition behavior typical of CO oxidation catalysts such as platinum particles supported on γ-Al_2O_3[21] and copper supported on SiO_2.[22] Thus, a sharp increase in conversion occurs at a temperature near 448 K for the supported rhodium and at a temperature near 523 K for the supported iridium catalyst. The activity of each catalyst after an induction period in the flow reactor was independent of whether it was initially in the form of the supported metal clusters or the supported metal oxide clusters formed by

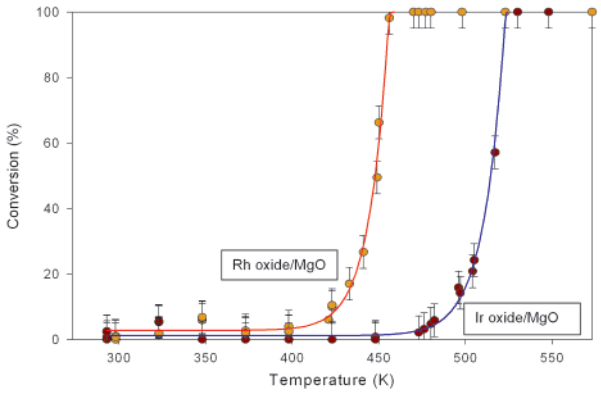

Figure 2. CO conversion under steady-state conditions catalyzed by iridium oxide and by rhodium oxide nanoclusters.

oxidation of the supported metal clusters. Thus, we suggest that the catalytically active species were likely the oxidized clusters. The activities of these catalysts for CO oxidation are similar to that of platinum particles supported on γ-Al_2O_3 under similar reaction conditions, for which the ignition behavior occurs at about 448 K.[21]

Acknowledgment. This research was supported by the U. S. Department of Energy, Office of Energy Research, Office of Basic Energy Sciences, Division of Chemical Sciences, Contract FG02-87ER13790. We acknowledge the support of the U. S. Department of Energy, Division of Materials Sciences, under Contract Number DE-FG05-89ER45384, for its role in the development and operation of beamline X-11A at the National Synchrotron Light Source (NSLS). The NSLS is supported by the Department of Energy, Division of Materials Sciences and Division of

Chemical Sciences, under Contract Number DE-AC02−76CH00016. EXAFS experiments were also performed at the Stanford Synchrotron Radiation Laboratory (SSRL), which is operated by Stanford University for the Department of Energy, Office of Basic Energy Sciences. The EXAFS data were analyzed with XDAP.[23]

References

(1) Vann, W. D.; Bell, R. C.; Castleman, A. W., Jr. *J. Phys. Chem. A* **1999**, *103*, 10846.
(2) Deutsch, S. E.; Miller, J. T.; Tomishige, K.; Iwasawa, Y.; Weber, W. A.; Gates, B. C. *J. Phys. Chem.* **1996**, *100*, 13408.
(3) Zhao, A.; Gates, B. C. *J. Am. Chem. Soc.* **1996**, *118*, 2458.
(4) Xu, Z.; Xiao, F.-S.; Purnell, S. K.; Alexeev, O.; Kawi, S.; Deutsch, S. E.; Gates, B. C. *Nature (London)* **1994**, *372*, 346.
(5) Carlsson, A.; Karlsson, G.; Bovin, J.-O.; Oku, T.; Okamoto, Y.; Ohnishi, N.; Terasaki, O. *Eur. Phys. J. D* **1999**, *9*, 623.
(6) Okamoto, Y.; Kobayashi, Y.; Imanaka, T. *Catal. Lett.* **1993**, *20*, 49.
(7) Moller, K.; Bein, T.; Ozkar, S.; Ozin, G. *J. Phys. Chem.* **1991**, *95*, 5276.
(8) Dossi, C.; Psaro, R.; Ugo, R. *J. Organomet. Chem.* **1988**, *353*, 259.
(9) Dufour, P.; Huang, L.; Choplin, A.; Sanchez-Delgado, R.; Theolier, A.; Basset, J.-M. *J. Organomet. Chem.* **1988**, *354*, 243.
(10) Argo, A. M., Ph.D. Dissertation, University of California, Davis, 2001.
(11) Panjabi, G.; Argo, A. M.; Gates, B. C. *Chem. Eur. J.* **1999**, *5*, 2417.
(12) Duivenvoorden, F. B. M.; Koningsberger, D. C.; Uh, Y. S.; Gates, B. C. *J. Am. Chem. Soc.* **1986**, *108*, 6254.
(13) Lu, D.; Rehr, J. J. *J. Phys. (Paris) C8* **1986**, *47*, 67.
(14) van Zon, F. B. M.; Maloney, S. D.; Gates, B. C.; Koningsberger, D. C. *J. Am. Chem. Soc.* **1993**, *115*, 10317.
(15) van Zon, J. B. A. D., Ph.D. Dissertation, Eindhoven University of Technology, The Netherlands, 1988.
(16) van Zon, J. B. A. D.; Koningsberger, D. C.; van't Blik, H. F. J.; Sayers, D. E. *J. Chem. Phys.* **1985**, *82*, 5742.
(17) Vaarkamp, M.; Linders, J. C.; Koningsberger, D. C. *Phys. B* **1995**, *209*, 159.
(18) Kirlin, P. S.; van Zon, F. B. M.; Koningsberger, D. C.; Gates, B. C. *J. Phys. Chem.* **1990**, *94*, 8439.
(19) Koningsberger, D. C.; Gates, B. C. *Catal. Lett.* **1992**, 14, 271.
(20) Abbet, S.; Riedo, E.; Brune, H.; Heiz, U.; Ferrari, A. M.; Giordano, L.; Pacchioni, G. *J. Am. Chem. Soc.* **2001**, 123, 6172.
(21) Kahlich, M. J.; Gasteiger, H. A.; Behm, R. J. *J. Catal.* **1997**, *171*, 93.
(22) Inui, T.; Ono, Y.; Takagi, Y.; Kim, J.-B. *Appl. Catal. A General* **2000**, *202*, 215.
(23) Vaarkamp, M. *Catal. Today* **1998**, 39, 271.

NL0155882